# Many-Body Interactions in Semiconductors Probed by Optical Two-Dimensional Fourier Transform Spectroscopy

Xiaoqin Li,[1] Tianhao Zhang,[1,2] Camelia N. Borca,[1] and Steven T. Cundiff[1]

[1]*JILA, University of Colorado and National Institute of Standards and Technology, Boulder, Colorado 80309-0440, USA*

[2]*Department of Physics, University of Colorado, Boulder, Colorado 80309-0320, USA*

(Received 3 August 2005; published 7 February 2006)

We study many-body interactions between excitons in semiconductors by applying the powerful technique of optical two-dimensional Fourier transform spectroscopy. A two-dimensional spectrum correlates the phase (frequency) evolution of the nonlinear polarization field during the initial evolution and the final detection period. A single two-dimensional spectrum can identify couplings between resonances, separate quantum mechanical pathways, and distinguish among microscopic many-body interactions.

DOI: 10.1103/PhysRevLett.96.057406 PACS numbers: 78.47.+p, 42.50.Hz, 81.07.Ta

An ideal model system for the investigation of many-body physics is an optically excited semiconductor, where excitonic resonances dominate the optical properties of direct-gap semiconductors near the fundamental band gap at low temperature [1,2]. An exciton is a quasiparticle consisting of a bound electron-hole pair. The part of the Coulomb interaction neglected in exciton formation leads to interactions among them.

Many-body interactions among excitons are commonly probed by nonlinear optical spectroscopy such as transient four-wave-mixing (FWM). However, conventional FWM techniques have several limitations. Following excitation by broadband ultrashort pulses, many electronic resonances could be excited simultaneously, leading to complicated oscillatory temporal evolution in FWM. It is difficult to distinguish whether such oscillations arise from polarization interference of uncoupled oscillators or quantum beats from coupled resonances [3–5]. In addition, many quantum mechanical pathways involving various relaxation times contribute to the FWM signal; an experimental approach capable of separating these contributions may allow more detailed dynamical information to be extracted. Furthermore, there is an intrinsic ambiguity regarding the microscopic mechanism of many-body interactions underlying the nonlinear response. The classic signature of exciton-exciton correlations in time-integrated (integrated over the detection period) two-pulse FWM experiments is the appearance of a signal at negative delays [6]. However, several microscopic interaction mechanisms can result in a negative-delay signal. These mechanisms are described phenomenologically as local fields [6], biexcitons [7], excitation-induced dephasing (EID) [8], or excitation-induced shift (EIS) [9]. The ambiguity among the interaction mechanisms primarily arises because FWM experiments only measure the intensity of the signal, thereby discarding important information encoded in the phase.

Following the revolutionary development in nuclear magnetic resonance [10], optical frequency two-dimensional (2D) Fourier transform spectroscopy has recently been implemented to study electronic and vibrational couplings in molecular systems [11–14]. We have chosen a prototypical system, GaAs multiple quantum wells, to demonstrate the feasibility and unique advantages of optical 2D Fourier transform spectroscopy as a new tool for studying many-body interactions in semiconductors. A single two-dimensional spectrum can identify couplings among resonances, separate quantum mechanical pathways, and distinguish among microscopic mechanisms for the many-body interactions by providing previously inaccessible phase information [15]. Thus, 2D Fourier transform spectroscopy poses exciting challenges to semiconductor many-body theory by imposing unprecedented constraints.

Two-dimensional Fourier transform spectroscopy is an enhanced FWM technique, which *monitors* and *correlates* nonlinear polarization phase evolution during two independent time periods, $\tau$ and $t$, separated by a mixing time, $T$, as illustrated in Fig. 1(a). A 2D spectrum as a function of the absorption frequency ($\omega_\tau$) and emission frequency ($\omega_t$) is then obtained by Fourier transforming the FWM signal with respect to time variables $\tau$ and $t$. The relation between driving fields, nonlinear polarization, FWM signal field, and 2D spectrum has been derived previously [13]. The signal field arises from the third order polarization

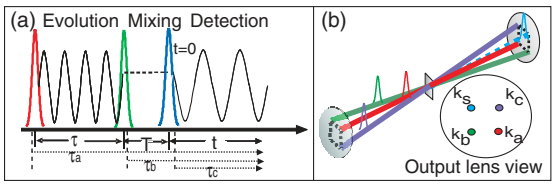


FIG. 1 (color). (a) Schematic of the excitation sequence showing the relevant time intervals. Note the dashed line indicating that the phase during time period $t$ is related to the phase evolution during time $\tau$. (b) Diagram showing geometry of excitation pulses and generated signal.

 

$$P^{(3)}(t,\tau,T) = \int_0^\infty \int_0^\infty \int_0^\infty S^{(3)}(\tau_a,\tau_b,\tau_c)E_a(t-\tau_a) \times E_b(t-\tau_b)E_c(t-\tau_c)d\tau_a d\tau_b d\tau_c, \quad (1)$$

which acts as a source term in Maxwell's equations. The third order impulsive response $S^{(3)}$ can be calculated. The interaction times $\tau_i$ relate to the incident pulse timings and the origin of the detection time ($t = 0$) is defined as the peak of the third pulse as indicated in Fig. 1(a). The real field in time is $E(t) = \hat{E}(t) + \hat{E}^*(t)$, where $\hat{E}(t) = (1/2) \times e(t)\exp(i\omega t)$. The frequency domain polarization $\hat{P}^{(3)}(\omega_t, \tau, T)$ is simply the Fourier transform with respect to $t$. The signal field radiated from this polarization is:

$$\hat{E}_{\text{sig}}(\omega_t,\tau,T) = \frac{2\pi l}{nc} i\omega_t \hat{P}^{(3)}(\omega_t,\tau,T), \quad (2)$$

where $l$ is the sample length, $c$ is the speed of light in vacuum, and $n$ is material index of refraction. 2D spectrum is then defined as the Fourier transform with respect to delay $\tau$:

$$S_{2D}(\omega_t,\omega_\tau,T) \equiv \int_0^\infty \hat{E}_{\text{sig}}(\omega_t,\tau,T)\exp(i\omega_\tau\tau)d\tau. \quad (3)$$

Experimentally, the FWM signal is completely characterized in amplitude and phase via spectral interferometry [16], where the FWM signal is heterodyne detected with a phase-stabilized reference pulse after passing through a spectrometer, yielding the emission axis $\omega_t$ directly. Characterization of the signal field includes not just the spectral phase, but the overall phase with respect to the third pulse, which is the appropriate reference for uniquely defining the phase of the signal field [17–20]. The indirect absorption frequency axis, $\omega_\tau$, is obtained by Fourier transform with respect to $\tau$. The experimental challenges mainly lie in the requirements to maintain phase stability ($\sim \frac{\lambda}{50}$) between multiple pulse pairs and step delay $\tau$ with subwavelength precision. We meet these requirements by implementing two actively stabilized interferometers [21].

In simple terms, the imaginary part of a 2D spectrum measures the transient change in the refractive index, while the real part approximates the resonant absorption of a probe field at frequency $\omega_t$, induced by the excitation frequency $\omega_\tau$. The proper decomposition of a 2D spectrum into real and imaginary parts relies on the comparison to an independent spectrally resolved differential transmission (SRDT) measurement. Experimentally, a constant phase rotation $e^{i\theta}$ is applied to the complex FWM signal obtained at $\tau = 0$, and $\theta$ is adjusted to minimize the difference between the real part of FWM and the SRDT spectrum at the same time $T$. Because the transmitted probe serves as a local oscillator in DT, it selects the real part of the signal field. Equivalently, one can compare the integration of the real part of a 2D spectrum along the absorption axis with the SRDT [22]. The second approach highlights the ability of a 2D spectrum to reveal the homogeneous line shape with high spectral resolution even in the presence of inhomogeneous broadening, which is not possible with SRDT.

The experimental setup is described in detail elsewhere [21]. As illustrated in Fig. 1(b), three collinearly polarized pulses are configured in the phase-matched "box" geometry. The signal is detected in the background free direction $\mathbf{k}_s = -\mathbf{k}_a + \mathbf{k}_b + \mathbf{k}_c$. The sample consists of ten periods of a 10 nm GaAs quantum well separated by 10 nm $Al_{0.3}Ga_{0.7}As$ barriers and is held at $\sim$10 K. As a result of quantum confinement, the two valence bands are energetically split by approximately 6 meV, resulting in two corresponding exciton resonances (heavy-hole and light-hole excitons) shown in Fig. 3(a). The linear absorption spectrum yields a heavy-hole exciton linewidth of $\sim$1.5 meV, due in part to inhomogeneous broadening from well-width fluctuations. At the excitation densities of $\sim 10^{10}$ excitons/well/cm$^2$, the homogeneous linewidth is $\sim$0.8 meV.

Based on the time ordering of the conjugated field, $\mathbf{k}_a$, both "rephasing" and "nonrephasing" experiments can be performed. For rephasing (or photon echo) measurements, $\mathbf{k}_a$ arrives first and the system evolves in conjugate frequencies during the time periods $\tau$ and $t$. The phase of the FWM signal is given by $e^{i(-\omega_\tau\tau+\omega_t t)}$ allowing cancellation of dephasing within an ensemble with inhomongeneously distributed oscillation frequencies. For nonrephasing (or virtual echo) measurements, $\mathbf{k}_a$ arrives second and the system has the same phase evolution direction during $\tau$ and $t$, i.e., $e^{i(\omega_\tau\tau+\omega_t t)}$. The different phase evolution during two time periods is further illustrated by the Feynman diagrams shown in Fig. 2. Feyman diagrams provide a convenient approach to keep track of all possible quantum mechanical paths to a given order of electric field in a perturbative expansion of the optical Bloch equations. For rephasing diagrams such as RA, the phase evolution of the polarization after the first pulse (01) and the third pulse (10) is opposite in sign. For nonrephasing diagrams such as NA, the phase evolution after the first pulse (10) and the third pulse (10) has the same sign. One cannot access nonrephasing pathways in commonly used two-beam self-diffracted FWM measurements. In general, nonrep-

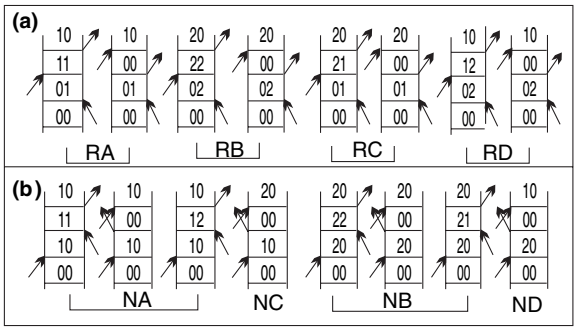


FIG. 2. Feynman diagrams for all possible quantum mechanical pathways for (a) rephasing and (b) nonrephasing measurements in a V system, where 0, 1, 2 corresponds to crystal ground state, heavy-hole, and light-hole excitons, respectively.

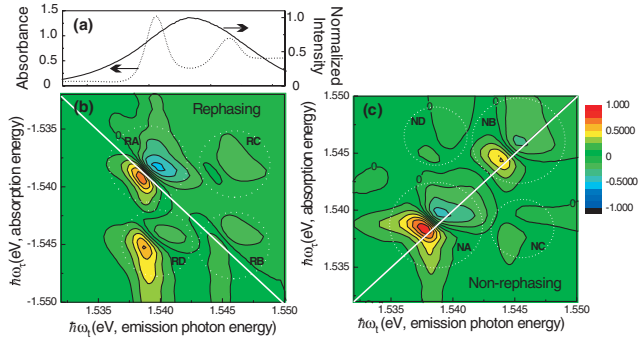


FIG. 3 (color). Linear absorption, excitation pulse spectrum (a) and experimental real spectra for the rephasing (b) and nonrephasing (c) pulse sequences. Both spectra in (b) and (c) are normalized to the most intense peak.

hasing measurements provide complementary information to rephasing measurements, such as resolving inhomogeneity and the degree of correlation of inhomogeneity between the coupled modes [23].

We present the measured rephasing and nonrephasing real spectra in Figs. 3(b) and 3(c), respectively. The phase evolution during the detection time, $t$, defines the sign of the frequencies. Thus rephasing processes produce signals with negative $\omega_\tau$ [Fig. 3(b)], whereas nonrephasing processes correspond to positive $\omega_\tau$ [Fig. 3(c)]. In Fig. 3(b), two diagonal peaks, RA and RB, correspond to the heavy-hole and light-hole excitons at 1.539 eV and 1.545 eV, respectively. The off-diagonal peaks (RC and RD) indicate oscillation frequency changes during or between the two time periods; thus the participating resonances must be coupled. The mixing time $T$ was set to 120 fs for data shown here to avoid other coherent orders when the excitation pulses temporally overlap. Separate measurements with $T = 0$ exhibited no qualitative difference (not shown). Therefore, the cross peaks arise from coherent coupling between the resonances as opposed to population relaxation observed in molecular systems [14]. For excitation pulses with collinear polarizations, the heavy-hole and light-hole exciton resonances are coupled through common conduction band states while different valence bands are involved. One can model the dynamics of the coupled resonances as a "V" system, which ignores the doubly excited (biexciton) states and polarization selection rules [7].

In order to understand the qualitative features of the 2D spectra, we refer to the Feynman diagrams in Fig. 2. All eight rephasing quantum mechanical pathways shown in Fig. 2(a) contribute in conventional FWM techniques detecting the intensity of the signal fields, leading up to 36 terms. By detecting the signal field itself and spreading the spectrum into two dimensions, 2D Fourier transform spectroscopy can separate different quantum mechanical pathways, yielding more detailed dynamic information. One can associate each peak in a 2D spectra to a small number of distinct quantum mechanical pathways depicted in Fig. 2. In the nonrephasing spectrum shown in Fig. 3(c), the relative intensities of the cross peaks (NC and ND) are weaker compared to Fig. 3(b) (RC and RD). This observation is consistent with the smaller number of diagrams contributing to the cross peaks in the nonrephasing measurements. The diagrams used in the microscopic semiconductor theory can be mapped with the Feynman diagrams shown in Fig. 2 and then decorated with interaction lines to take into account Coulomb correlations [24].

The dominance of "dispersive" line shapes (the derivative of a peak) of both the diagonal and cross peaks qualitatively contradicts the prediction of a simple theory for phase space filling. We numerically solve the modified optical Bloch equations of a V system [9] to reproduce these distinct line shapes. It is instructive to examine the equation of motion for the off-diagonal term of the density matrix, $\rho_{12}$, for a two-level system that includes both excitation-induced dephasing (EID) and excitation-induced shift (EIS) effects,

$$\dot{\rho_{12}} = -(\gamma_0 + \gamma' N\rho_{22})\rho_{12} + i(\omega_0 + \omega' N\rho_{22})\rho_{12} + \frac{i}{\hbar}\mu_{12}E(\rho_{22} - \rho_{11}), \quad (4)$$

where $\rho_{11}$ and $\rho_{22}$ denote the ground state and excited state population, respectively, $\mu_{12}$ is the dipole moment, $E$ is the electric field amplitude, and $N$ is the number density of oscillators. The signal polarization is proportional to $\rho_{12}$. The excitation density-dependent dephasing rate ($\gamma_0 + \gamma' N\rho_{22}$) and resonance frequency ($\omega_0 + \omega' N\rho_{22}$) model many-body interactions. The linear dependence of the dephasing rate and resonance frequency on excitation density is a good approximation in the low power regime. Note that the excitation-induced dephasing ($-\gamma' N\rho_{22}\rho_{12}$) and shift ($i\omega' N\rho_{22}\rho_{12}$) terms modify the nonlinear signal differently due to the phase shift introduced by the constant $i$. Therefore, phase-sensitive measurements can *directly* address this critical distinction between different mechanisms, whereas intensity measurements cannot [8,25,26]. Furthermore, 2D spectroscopy can make a distinction between EID and EIS even in the presence of inhomogeneous broadening, which can be difficult using other techniques.

The calculated real spectra for only the rephasing pulse sequence without many-body interactions and with EID are shown in Figs. 4(a) and 4(b), respectively. In both cases, the real parts of the spectra display dominant "absorptive" line shapes, i.e., a peak, inconsistent with experimental data. However, if EIS is included, the calculated spectra [Figs. 5(a) and 5(b)] qualitatively match the measured ones [Figs. 3(b) and 3(c)]. We note that the peak intensity of RC is weaker compared to that of RD in Fig. 3(b). This feature may be attributed unequal EID or different dephasing times between the heavy- and light-hole excitons. Although our goal is not quantitative determination of phenomenological parameters, we note that they are in reasonable agreement with previous studies [9].

There has been significant progress in theoretical understanding of manifestation of exciton correlations in optical nonlinear response [1,24,27–29]. Different microscopic

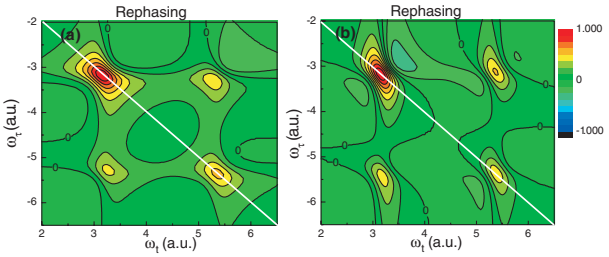


FIG. 4 (color). Calculated real spectra for the rephasing sequence. (a) is based on a simple V system without any many-body interactions, while excitation-induced dephasing is included in (b).

approaches in terms of density matrices as well as nonequilibrium Green's functions have been developed. Within the density matrix approach, Coulomb interaction leads to an infinite hierarchy of higher order of density matrices, which can be truncated using either correlation expansion or dynamics controlled truncation scheme. Within the Green's function approach, the problem of an infinite hierarchy is deferred to constructing the self-energy. EID and EIS correspond to renormalization of the imaginary and real parts of the exciton self-energy. Therefore, they cannot be treated as independent parameters in a microscopic theory. Whether or not modeling 2D spectra based on a full microscopic theory requires further refinement of existing theoretical concepts remains to be explored.

In summary, we have demonstrated that optical 2D Fourier transform spectroscopy offers the following advantages. (1) By correlating polarization phase evolution in two independent time periods, coupling between different resonances can be identified even in the case of a congested spectrum [30]. (2) Contributions from different quantum mechanical pathways are separated and associated with different peaks in a 2D spectrum. (3) Sensitivity to phase information distinguishes between different microscopic mechanisms of many-body correlations. Optical 2D Fourier transform spectroscopy is still in its early development. Detailed experimental studies and comparison between the experiments and microscopic calculations have yet to be performed. In view of the conceptual advantages it offers over conventional FWM technique, multidimensional Fourier transform spectroscopy is expected to develop into a powerful tool for probing electron dynamics and many-body correlations in various systems including both large molecules and semiconductors.

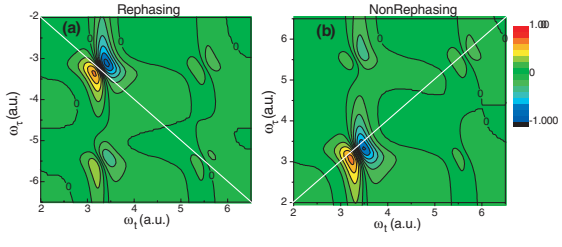


FIG. 5 (color). Calculated real spectra for the rephasing (a) and nonrephasing (b) pulse sequences based on a V system with excitation-induced shift included.

The authors gratefully acknowledge D. M. Jonas, M. DeCamp, and L. J. Sham for enlightening discussions. This work is supported by DOE/BES and NSF.

[1] H. Haug and S. W. Koch, *Quantum Theory of the Optical and Electronic Properties of Semiconductors* (World Scientific, Singapore, 2004).
[2] D. S. Chemla and J. Shah, Nature (London) **411**, 549 (2001).
[3] Various methods used to distinguish quantum beats and polarization interference, including time resolved FWM, can be model dependent. See Refs. [4,5].
[4] M. Koch *et al.*, Phys. Rev. Lett. **69**, 3631 (1992).
[5] X. Zhu *et al.*, Phys. Rev. Lett. **73**, 209 (1994).
[6] K. Leo *et al.*, Phys. Rev. Lett. **65**, 1340 (1990).
[7] K. Bott *et al.*, Phys. Rev. B **48**, 17 418 (1993).
[8] H. Wang *et al.*, Phys. Rev. Lett. **71**, 1261 (1993).
[9] J. M. Shacklette and S. T. Cundiff, Phys. Rev. B **66**, 045309 (2002).
[10] R. R. Ernst, G. Bodenhausen, and A. Wokaun, *Principles of Nuclear Magnetic Resonance in One and Two Dimensions* (Oxford Science Publications, New York, 1987).
[11] S. Mukamel, Annu. Rev. Phys. Chem. **51**, 691 (2000).
[12] D. M. Jonas, Annu. Rev. Phys. Chem. **54**, 425 (2003).
[13] J. D. Hybl *et al.*, J. Chem. Phys. **115**, 6606 (2001).
[14] T. Brixner *et al.*, Nature (London) **434**, 625 (2005).
[15] C. N. Borca *et al.*, Chem. Phys. Lett. **416**, 311 (2005).
[16] L. Lepetit *et al.*, J. Opt. Soc. Am. B **12**, 2467 (1995).
[17] Many researchers have realized the importance of characterizing the complete nonlinear polarization generated in semiconductors. However, previous experiments failed to explore the full potential of 2D FT spectroscopy due to the lack of phase control between excitation pulses or the inability to separate the real and imaginary parts. See Refs. [18–20].
[18] J. Y. Bigot *et al.*, Phys. Rev. Lett. **70**, 3307 (1993).
[19] X. Chen *et al.*, Phys. Rev. B **56**, 9738 (1997).
[20] J. P. Likforman *et al.*, Opt. Lett. **22**, 1104 (1997).
[21] T. H. Zhang *et al.*, Opt. Express **13**, 7432 (2005).
[22] S. M. Gallagher Faeder and D. M. Jonas, J. Phys. Chem. **103**, 10 489 (1999).
[23] N. Demirdoven *et al.*, Phys. Rev. Lett. **89**, 237401 (2002).
[24] M. Z. Maialle and L. J. Sham, Phys. Rev. Lett. **73**, 3310 (1994).
[25] EID and EIS have been studied by measuring excitation power dependent dephasing times or line shifts in various FWM and pump-probe experiments. See Refs. [8,26].
[26] T. Guenther *et al.*, Phys. Rev. Lett. **89**, 057401 (2002).
[27] V. M. Axt and A. Stahl, Z. Phys. B **93**, 195 (1994).
[28] C. Sieh *et al.*, Eur. Phys. J. B **11**, 407 (1999).
[29] V. M. Axt and T. Kuhn, Rep. Prog. Phys. **67**, 433 (2004).
[30] A previous study by A. Euteneuer *et al.* [Phys. Rev. Lett. **83**, 2073 (1999)] is based on similar ideas. However, phase information was not obtained since FWM intensity was measured.